

A BOUNDARY INTEGRAL FORMULATION OF AN ACOUSTIC BOUNDARY LAYER MODEL IN 2D

JACOB LINDEN, TRAVIS ASKHAM, AND JEREMY HOSKINS

ABSTRACT. We present a boundary integral formulation of the Helmholtz equation with visco-thermal boundary conditions, in two dimensions. Such boundary conditions allow for the accurate simulation of viscous and thermal losses in the vicinity of the boundary, which are particularly relevant in acoustic devices with narrow features. Using cancellations between hyper-singular operators, a variant of the method of images technique, and analytic preconditioners, we derive integral equations that are Fredholm second-kind, up to the application of a boundedly invertible operator. This approach allows for the fast and accurate solution of acoustics problems with boundary layers.

1. INTRODUCTION

While wave equation (or Helmholtz equation, for time harmonic waves) and acoustic ray models are common in acoustic wave propagation, the effects of the fluid medium must be taken into account to obtain an accurate model in certain regimes. In particular, viscous and thermal effects are significant in a variety of acoustic devices with narrow regions, including hearing aids [1, 2], micro-electro-mechanical systems [3, 4, 5], metamaterials [6, 7, 8, 9], perforated panels [10, 11, 12], and phase plugs [13, 14, 15]. There is a large body of recent work on the design and optimization of such devices [16, 17, 18, 19, 20, 21, 22], and, more generally, the simulation of visco-thermal effects [23, 24, 25, 26, 27, 28]. Many of these studies model acoustic waves using the linearized Navier-Stokes equations, or simplifications thereof, and solve the equations by boundary element and finite element methods.

Because viscous and thermal losses mostly occur in narrow boundary layers, it is appealing to model acoustic waves in such devices by enforcing the Helmholtz equation in the bulk and accounting for the losses through an effective boundary condition. In [29], a boundary layer analysis was used to derive an effective boundary condition for visco-thermal effects of the form

$$(1) \quad c_1 \Delta_\Gamma u + c_2 u + \partial_n u = f,$$

where Δ_Γ denotes the Laplace-Beltrami operator on the boundary, ∂_n denotes the normal derivative, and c_1 and c_2 are constants depending on the frequency, specific heat capacities, and boundary layer thicknesses. The authors of [29] then

(JL) COMPUTATIONAL AND APPLIED MATHEMATICS, UNIVERSITY OF CHICAGO
 (TA) DEPARTMENT OF MATHEMATICAL SCIENCES, NEW JERSEY INSTITUTE OF TECHNOLOGY
 (JH) COMPUTATIONAL AND APPLIED MATHEMATICS, UNIVERSITY OF CHICAGO, AND NSF-SIMONS NATIONAL INSTITUTE FOR THEORY AND MATHEMATICS IN BIOLOGY

E-mail addresses: jacoblinden@uchicago.edu, askham@njit.edu,
jeremyhoskins@uchicago.edu.

Date: January 27, 2026.

verified the model against simulations of the full linearized Navier-Stokes equations in a phase plug geometry and found good agreement. Boundary conditions of this form have appeared in other wave propagation applications, where they are known as generalized impedance boundary conditions [30, 31, 32, 33, 34] or *Wentzell* boundary conditions [35, 36].

Boundary integral methods present several advantages for the solution of the Helmholtz equation, particularly for problems in complicated geometries. These methods represent the solution throughout the domain as a layer potential induced by a density defined on the boundary alone, so that only the boundary of the domain needs to be discretized and fewer degrees of freedom can be used to resolve a given problem. Depending on the boundary condition, an appropriate layer potential representation can be designed so that the density is determined by a Fredholm second-kind integral equation. In this case, the numerical approximations of the integral equation for the density remain well-conditioned under refinement of the boundary discretization. Such representations are also useful analytically in establishing the existence and uniqueness of solutions, characterizing the nullspaces when the equations are not invertible, and analyzing solutions in singular geometries. While we do not seek to review the literature here, see [37, 38, 39, 40, 41] and the references therein for more on the theory and practice of boundary integral methods.

In this work, we construct and analyze a novel boundary integral equation formulation of the Helmholtz equation with the boundary condition (1). The method is based on a particular combined field representation of the pressure and an analytic surface pre-conditioner, resulting in an integral equation for the density that is Fredholm second-kind. We show that this representation can also be modified to handle “domain decomposition” problems, as in [29], where the boundary layer condition (1) is imposed in a wave guide and impedance conditions are imposed on artificial curves that enclose the ends. Using an image method, it is possible to again obtain an integral equation that is Fredholm second kind. Our representations are amenable to standard integral equation methods for their discretization and efficient solution and the techniques for deriving the representations apply more broadly to generalized impedance boundary conditions of this type. We demonstrate the effectiveness and properties of the representation through several numerical simulations.

2. BACKGROUND

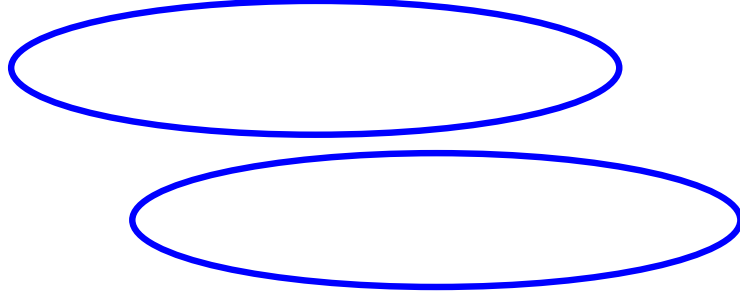
2.1. Description of the geometry. Consider a region Ω (not necessarily bounded) with positively oriented boundary $\Gamma := \partial\Omega$ of finite length. In this paper we treat the following two classes of problems.

Case I: The boundary Γ is smooth, and visco-thermal boundary conditions are imposed on the entire boundary. In this case, we denote $\Gamma = \Gamma_*$. An example is given in Figure 1a.

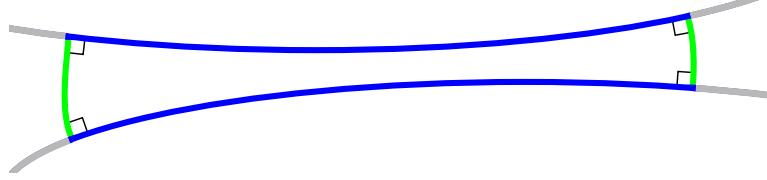
Case II: The boundary Γ is the union of two collections of smooth, disjoint planar curves Γ_* and Γ_\circ . We impose the additional assumptions that Γ_* and Γ_\circ intersect at right angles, and that the curvature of Γ_\circ vanishes at its boundary. Visco-thermal boundary conditions are imposed on Γ_* and Robin boundary conditions are imposed on Γ_\circ . Though in principle Γ_\circ could represent a physical surface, our main motivation is domain decomposition, where the solutions in adjacent regions are coupled together using impedance-to-impedance maps (see section 3.4).

In this context, the freedom to choose Γ_o enables our imposition of the additional constraints.

For simplicity we assume in the sequel that Γ_* and Γ_o are each the union of two disjoint curves: $\Gamma_* = \Gamma_*^1 \cup \Gamma_*^2$ and $\Gamma_o = \Gamma_o^1 \cup \Gamma_o^2$. However, our method easily extends to treat arbitrary (finite) numbers of connected components. An example geometry is given in Figure 1b.



(A) Case I: the boundary Γ is a smooth curve or union of smooth curves, on which visco-thermal boundary conditions are imposed. In this case, we denote $\Gamma = \Gamma_*$.



(B) Case II: Γ is the union of Γ_* (blue) and a fictitious boundary Γ_o (green).

FIGURE 1

2.2. Modeling boundary layers as a boundary condition. We denote the viscous and thermal acoustic boundary layer thicknesses by δ_V and δ_T respectively. These quantities depend in particular on the frequency ω , and typically lie in the range of $20 - 400 \mu\text{m}$ for audible sound [29]. The wave number is $k = \omega/c$, where c is the speed of sound. The constant $\gamma \geq 1$ will denote the ratio of the specific heat capacities at constant pressure and constant volume. We define the coefficients

$$(2) \quad c_1 = -\delta_V \frac{i-1}{2},$$

$$(3) \quad c_2 = \delta_T k^2 (\gamma - 1) \frac{i-1}{2}.$$

Assuming that the minimal radius of curvature in Γ_* far exceeds the boundary layer thicknesses, we consider the following boundary value problem for the acoustic

pressure u [29]:

$$(4) \quad \begin{cases} \Delta u + k^2 u = 0 & \Omega, \\ c_1 \Delta_\Gamma u + c_2 u + \partial_n u = f & \Gamma_*, \\ a u + \partial_n u = g & \Gamma_0, \\ \partial_b u = h & \partial\Gamma_*. \end{cases}$$

Here a is a complex constant, Δ_Γ denotes the Laplace-Beltrami operator, and ∂_n , ∂_b denote the normal and binormal derivatives respectively.

The PDE (4) is used in Case II, while in Case I, Γ_0 and $\partial\Gamma_*$, and their associated boundary conditions, are omitted. In Case I, if Ω is an exterior domain then an additional (outgoing) radiation condition at infinity is imposed:

$$(5) \quad \lim_{|x| \rightarrow \infty} \frac{x}{|x|} \cdot \nabla u(x) - iku(x) = o\left(\frac{1}{\sqrt{|x|}}\right).$$

2.3. Mathematical preliminaries. The (outgoing) free space Green's function for the Helmholtz equation in two dimensions is given by

$$(6) \quad G(x, y) = \frac{i}{4} H_0^{(1)}(k|x - y|),$$

where $H_0^{(1)}$ is the zeroth order Hankel function of the first kind (see [42, (10.2.5)]), and satisfies the PDE

$$(7) \quad \Delta_x G(x, y) + k^2 G(x, y) = \delta(x - y),$$

together with the radiation condition (5).

Given a piecewise smooth curve Γ , the *single layer* and *double layer* operators are defined, respectively, by

$$(8) \quad S[\sigma](x) = \int_\Gamma G(x, y) \sigma(y) \, ds(y),$$

$$(9) \quad D[\sigma](x) = \int_\Gamma [\partial_{n_y} G(x, y)] \sigma(y) \, ds(y),$$

where n_y denotes the outward normal vector at $y \in \Gamma$ and $\partial_n = n \cdot \nabla$ denotes the normal derivative. For $\sigma \in L^2(\Gamma)$, (8) and (9) automatically satisfy the Helmholtz equation in $\mathbb{R}^2 \setminus \Gamma$. For the evaluation of the single and double layer potentials on surface, i.e. for $x \in \Gamma$, we use the notations $S[\sigma]$ and $D[\sigma]$, respectively. We will also need the on-surface normal derivatives of S and D , defined as follows:

$$(10) \quad S'[\sigma](x) = \int_\Gamma [\partial_{n_x} G(x, y)] \sigma(y) \, ds(y),$$

$$(11) \quad D'[\sigma](x) = \int_\Gamma [\partial_{n_x} \partial_{n_y} G(x, y)] \sigma(y) \, ds(y),$$

for all $x \in \Gamma$. Note that $\partial_{n_x} \partial_{n_y} G$ is not integrable on Γ , so the integral defining the hypersingular operator D' is interpreted in the Hadamard finite part sense [40]. We will also use the notation S'' and D'' for the analogous operators with two normal derivatives on the x variables, whose integrals must also be interpreted in the finite part sense [43].

For $x \in \Gamma$ not a corner point, the operators D and S' satisfy the following standard jump relations:

$$(12) \quad \lim_{h \rightarrow 0} D[\sigma](x \pm hn_x) = \pm \frac{\sigma(x)}{2} + \mathcal{D}[\sigma](x),$$

$$(13) \quad \lim_{h \rightarrow 0} n_x \cdot \nabla S[\sigma](x \pm hn_x) = \mp \frac{\sigma(x)}{2} + \mathcal{S}'[\sigma](x).$$

The operators S and D' are continuous across Γ :

$$(14) \quad \lim_{h \rightarrow 0} S[\sigma](x \pm hn_x) = \mathcal{S}[\sigma](x),$$

$$(15) \quad \lim_{h \rightarrow 0} n_x \cdot \nabla D[\sigma](x \pm hn_x) = \mathcal{D}'[\sigma](x).$$

The operators \mathcal{S} , \mathcal{D} , and \mathcal{S}' are bounded from $L^2(\Gamma)$ to itself, while \mathcal{D}' is bounded from $H^1(\Gamma)$ to $L^2(\Gamma)$. If Γ is smooth, then \mathcal{S} , \mathcal{D} , and \mathcal{S}' are compact on $L^2(\Gamma)$ [44]. For domains with corners, though \mathcal{S} remains compact on $L^2(\Gamma)$, both \mathcal{D} and \mathcal{S}' are merely bounded in the vicinity of each corner [45].

3. INTEGRAL EQUATION FORMULATION

To obtain an integral representation for problems with the visco-thermal boundary condition (1), we first derive several properties of the Laplace-Beltrami operator applied to the standard Helmholtz layer potentials in Section 3.1. Then, we describe a representation for (1) on a single curve in isolation that leverages cancellations between hypersingular operators, along with an analytic preconditioning strategy, in Section 3.2. For a closed curve, as in Case I, these techniques are sufficient to obtain a Fredholm second kind equation. For an open curve with boundary conditions on the binormal data, as in Case II, the derivation is formal, as modifications of the layer potentials are required to ensure that some of the operators are well-defined. These issues are treated along with the full mixed boundary value problem for Case II in Section 3.3, which makes use of an extension of the method of images. Finally, we discuss the use of impedance-to-impedance maps for domain decomposition in this context in Section 3.4.

3.1. The Laplace-Beltrami operator and Helmholtz layer potentials. Consider a smooth, possibly open, planar curve Γ . For $h > 0$, let

$$(16) \quad \Gamma_h = \{x - hn_x : x \in \Gamma\}.$$

We further require h to be sufficiently small so that Γ_h does not self-intersect. We then define the operators

$$(17) \quad \mathcal{S}_{\Gamma_h, \Gamma} : L^2(\Gamma) \rightarrow L^2(\Gamma_h),$$

$$(18) \quad \mathcal{D}_{\Gamma_h, \Gamma} : L^2(\Gamma) \rightarrow L^2(\Gamma_h),$$

by the restriction of the usual layer potentials for densities on Γ to Γ_h . The curvature on Γ is defined by

$$(19) \quad \kappa = \nabla_\Gamma \cdot n.$$

The following lemma is a variation of a fact found, for example, in [46]:

Lemma 3.1. *Suppose that Γ is a smooth curve and $\sigma \in H^1(\Gamma)$. Then*

$$(20) \quad \lim_{h \rightarrow 0} \Delta_\Gamma \mathcal{S}_{\Gamma_h, \Gamma}[\sigma] = \Delta_\Gamma \mathcal{S}[\sigma] = -k^2 \mathcal{S}[\sigma] - \kappa \mathcal{S}'[\sigma] - \mathcal{S}''[\sigma].$$

Proof. The Laplacian can be decomposed as

$$(21) \quad \Delta = \Delta_\Gamma + \kappa \partial_n + \partial_n^2.$$

Proof of this fact can be found, for example, in [47]. Since $S[\sigma]$ satisfies the Helmholtz equation in $\mathbb{R}^2 \setminus \Gamma$,

$$(22) \quad \Delta_\Gamma \mathcal{S}_{\Gamma_h, \Gamma}[\sigma] = -k^2 \mathcal{S}_{\Gamma_h, \Gamma}[\sigma] - \kappa_h \mathcal{S}'_{\Gamma_h, \Gamma}[\sigma] - \mathcal{S}''_{\Gamma_h, \Gamma}[\sigma],$$

where κ_h denotes the curvature on Γ_h . The operator S is continuous across Γ in the sense of (14). The jump of \mathcal{S}' is given in (13). The following formula for the jump of \mathcal{S}'' is derived in [43]:

$$(23) \quad \lim_{h \rightarrow 0} \mathcal{S}''_{\Gamma_h, \Gamma}[\sigma] = -\frac{\kappa}{2} \sigma + \mathcal{S}''[\sigma].$$

Thus the jump terms of \mathcal{S}' and \mathcal{S}'' cancel, yielding the claim. \square

The following lemma gives a similar result for the double layer potential.

Lemma 3.2. *Suppose that Γ is a smooth curve and $\sigma \in H^2(\Gamma)$. Then*

$$(24) \quad \lim_{h \rightarrow 0} \Delta_\Gamma \mathcal{D}_{\Gamma_h, \Gamma}[\sigma] = \Delta_\Gamma \lim_{h \rightarrow 0} \mathcal{D}_{\Gamma_h, \Gamma}[\sigma] = -\frac{1}{2} \Delta_\Gamma \sigma + K[\sigma],$$

where the operator

$$(25) \quad K = -k^2 \mathcal{D} - \kappa \mathcal{D}' - \mathcal{D}''$$

has logarithmically singular kernel.

Proof. The proof is given in Appendix A. \square

3.2. An integral representation on Γ_*^j . Consider a single curve, Γ_*^j , on which we impose the acoustic boundary layer condition (1). To obtain a Fredholm second kind formulation of this problem, we use a particular linear combination of S and D constructed to cancel singularities, reducing the problem to an integro-differential equation on the boundary Γ_*^j . The resulting integro-differential equation is of a convenient form that lends itself easily to preconditioning.

Substituting the representation $u = S[\sigma]$ into the boundary condition on Γ_*^j and using Lemma 3.1 gives the expression

$$(26) \quad c_1 \Delta_\Gamma \mathcal{S}[\sigma] + c_2 \mathcal{S}[\sigma] + \left(\frac{I}{2} + \mathcal{S}' \right) [\sigma].$$

The operator $\Delta_\Gamma \mathcal{S}$ is hypersingular. On the other hand, if we use the representation $u = D[\sigma]$ then Lemma 3.2 yields

$$(27) \quad c_1 \Delta_\Gamma \left(-\frac{I}{2} + \mathcal{D} \right) [\sigma] + c_2 \left(-\frac{I}{2} + \mathcal{D} \right) [\sigma] + \mathcal{D}'[\sigma].$$

Though the operator \mathcal{D}' is also hypersingular, we note that the leading order singularities of \mathcal{D}' and \mathcal{S}'' in the sum $\mathcal{D}' + \mathcal{S}''$ cancel, and what remains is a continuous kernel. Applying Lemma 3.1, we find that

$$(28) \quad \mathcal{D}' - \Delta_\Gamma \mathcal{S} = (\mathcal{D}' + \mathcal{S}'') + \kappa \mathcal{S}' + k^2 \mathcal{S}.$$

Thus, taking the representation

$$(29) \quad u = \left(\mathcal{D} - \frac{1}{c_1} \mathcal{S} \right) [\sigma]$$

cancels the leading order singularities of $\Delta_\Gamma \mathcal{S}$ and \mathcal{D}' from (26) and (27). Substituting this into the boundary conditions yields, after some manipulations, the integro-differential equation

$$(30) \quad f = \left[-\frac{c_1}{2} \left(\Delta_\Gamma + \frac{1+c_1c_2}{c_1^2} I \right) + (c_1 \Delta_\Gamma + c_2 I) \mathcal{D} + c_2 \left(-\frac{I}{2} + \mathcal{D} \right) + (\mathcal{D}' + \mathcal{S}'') + k^2 \mathcal{S} + \kappa \mathcal{S}' - \frac{c_2}{c_1} \mathcal{S} - \frac{1}{c_1} \left(\frac{I}{2} + \mathcal{S}' \right) \right] [\sigma].$$

Next, we define the *surface wave number* on Γ_* as

$$(31) \quad k_\Gamma = \sqrt{\frac{1+c_1c_2}{c_1^2}},$$

with the branch of the square root taken such that $\Im k_\Gamma > 0$ (strict positivity is guaranteed by the form of c_1 and c_2) and we define a Helmholtz–Beltrami operator \mathcal{L} on Γ_* by

$$(32) \quad \mathcal{L} = \Delta_\Gamma + k_\Gamma^2 I.$$

We note that on a curve, the Laplace–Beltrami operator is the same as the second derivative with respect to arc length. In the following we let \mathcal{L}_j denote the restriction of \mathcal{L} to Γ_*^j . The surface Green’s function associated with \mathcal{L}_j is, therefore,

$$(33) \quad G_\Gamma^j(s, s') = \frac{1}{2ik_\Gamma} e^{ik_\Gamma |s-s'|} + \psi_j(s, s'),$$

where s, s' denote arc length, and ψ_j is smooth in s and s' separately and satisfies

$$(34) \quad \mathcal{L}_j \psi_j(s, s_0) = \mathcal{L}_j \psi_j(s_0, s') = 0,$$

for every $s_0 \in [0, L]$, where L is the length of Γ_*^j . Let

$$(35) \quad \mathcal{G}_j[\sigma](s) = \int_{\Gamma_*^j} G_\Gamma^j(s, s') \sigma(s') ds'.$$

Standard ODE results give that $\mathcal{G}_j : L^2(\Gamma_*^j) \rightarrow H^2(\Gamma_*^j)$ is bounded.

3.2.1. *Closed Γ_*^j .* Suppose now that Γ_*^j is a smooth, closed curve. In this case, the periodic Green’s function is desired, so in (33) we take

$$(36) \quad \psi_j(s, s') = \frac{1}{2ik_\Gamma} \sum_{\ell \neq 0} e^{ik_\Gamma |s-s'-\ell L|}.$$

For $\Im k_\Gamma > 0$, as is the case for the physical values of c_1 and c_2 in (2) and (3), the above series is absolutely convergent. For $\varphi \in H^2(\Gamma_*^j)$, integration by parts on Γ_*^j yields

$$(37) \quad \mathcal{G}_j \mathcal{L}_j \varphi = \varphi.$$

Noting that

$$(38) \quad c_1 \Delta_\Gamma + c_2 I = c_1 \mathcal{L} - c_1^{-1} I,$$

from (30) one obtains

$$(39) \quad \mathcal{G}_j f = \left[-\frac{c_1}{2} I + c_1 \mathcal{D} - \frac{1}{c_1} \mathcal{G}_j \mathcal{D} + \mathcal{G}_j (\mathcal{D}' + \mathcal{S}'') + \left(k^2 - \frac{c_2}{c_1} \right) \mathcal{G}_j \mathcal{S} \right]$$

$$+ \mathcal{G}_j \left(\kappa - \frac{1}{c_1} \right) \mathcal{S}' \right] \sigma.$$

The integral operator in the above equation is Fredholm second-kind on $H^2(\Gamma_*^j)$.

3.2.2. *Open Γ_*^j .* To obtain an integral equation on an open Γ_*^j , we proceed as in the previous section, except that further work is required to address the additional boundary conditions. We define

$$(40) \quad F_j[\varphi](s) = G_\Gamma^j(s, L)\varphi'(L) - G_\Gamma^j(s, 0)\varphi'(0).$$

Lemma 3.3. *The operator F_j is compact on $H^2(\Gamma_*^j)$.*

Proof. Since the embedding $H^2(\Gamma_*^j) \subset C^1(\Gamma_*^j)$ is continuous [48], the functionals

$$(41) \quad \varphi \mapsto \varphi'(0),$$

$$(42) \quad \varphi \mapsto \varphi'(L)$$

are bounded on $H^2(\Gamma_*^j)$. The range of F_j is a two-dimensional subspace of $C^\infty(\Gamma_*^j)$, and in particular of $H^2(\Gamma_*^j)$. Hence F_j is a bounded operator on $H^2(\Gamma_*^j)$ with finite-dimensional range, so it is compact. \square

We select ψ_j in (33) such that G_Γ^j is the Green's function with zero Neumann boundary conditions, i.e. $\partial_{s'} G_\Gamma^j(s, L)$ and $\partial_{s'} G_\Gamma^j(s, 0)$ are identically zero. Integration by parts on Γ_*^j then yields, for $\varphi \in H^2(\Gamma_*^j)$,

$$(43) \quad \mathcal{G}_j \mathcal{L}_j \varphi = (I + F_j)\varphi.$$

Let f_j and σ_j denote the restrictions of f and σ to Γ_*^j . Using (38), from (30) one obtains a non-periodic analogue of (39):

$$(44) \quad \mathcal{G}_j f_j = \left[-\frac{c_1}{2} I + c_1 \mathcal{D} - \frac{1}{c_1} \mathcal{G}_j \mathcal{D} + \mathcal{G}_j (\mathcal{D}' + \mathcal{S}'') + \left(k^2 - \frac{c_2}{c_1} \right) \mathcal{G}_j \mathcal{S} \right. \\ \left. + \mathcal{G}_j \left(\kappa - \frac{1}{c_1} \right) \mathcal{S}' + c_1 F_j \left(-\frac{I}{2} + \mathcal{D} \right) \right] \sigma.$$

The operator

$$(45) \quad \mathcal{R} = \frac{1}{c_1} \mathcal{D} + (\mathcal{D}' + \mathcal{S}'') + \left(k^2 - \frac{c_2}{c_1} \right) \mathcal{S} + \left(\kappa - \frac{1}{c_1} \right) \mathcal{S}'$$

has logarithmically singular kernel, and is thus compact on $L^2(\Gamma_*^j)$. The embedding

$$(46) \quad H^2(\Gamma_*^j) \xhookrightarrow{\iota} L^2(\Gamma_*^j)$$

is compact [48, 49], so the composition $\mathcal{G}_j \circ \mathcal{R} \circ \iota$ is compact on $H^2(\Gamma_*^j)$. Since the most singular part of the kernel of \mathcal{D} is $\mathcal{O}(r^2 \log r)$, \mathcal{D} is compact on $H^2(\Gamma_*^j)$. The operator F_j is compact by Lemma 3.3, so this proves that the operator applied to σ in (44) is Fredholm second kind on $H^2(\Gamma_*^j)$.

The operator has non-trivial cokernel because its range is contained in the range of \mathcal{G}_j , which only contains functions with zero Neumann data. This deficiency is related to the binormal boundary conditions, which must still be imposed.

For this representation, the binormal boundary conditions take the form

$$(47) \quad -\frac{1}{2}\sigma'(L) + \partial_s(\mathcal{D}\sigma)(L) - \frac{1}{c_1}\partial_s(\mathcal{S}\sigma)(L) = h_+,$$

$$(48) \quad -\frac{1}{2}\sigma'(0) + \partial_s(\mathcal{D}\sigma)(0) - \frac{1}{c_1}\partial_s(\mathcal{S}\sigma)(0) = -h_-.$$

Unfortunately, the value of $\partial_s(\mathcal{S}\sigma)$ is not necessarily defined at the end points. We will see how to modify the definition of S to alleviate this issue in the next subsection. For now, we proceed formally.

Multiplying (47) by $G_\Gamma^j(s, L)$, multiplying (48) by $G_\Gamma^j(s, 0)$, and taking the difference of the two yields

$$(49) \quad F_j \left(-\frac{I}{2} + \mathcal{D} \right) \sigma = \frac{1}{c_1} F_j \mathcal{S} \sigma + G_\Gamma^j(s, L) h_+ + G_\Gamma^j(s, 0) h_-.$$

Since $G_\Gamma^j(s, L)$ and $G_\Gamma^j(s, 0)$ are linearly independent, imposing this is equivalent to imposing (47) and (48). Substituting (49) back into (44) yields the following (formal) integral equation:

$$(50) \quad \tilde{f}_j = \left(-\frac{c_1}{2} I + c_1 \mathcal{D} - \frac{1}{c_1} \mathcal{G}_j \mathcal{D} + \mathcal{G}_j (\mathcal{D}' + \mathcal{S}'') \right. \\ \left. + \left(k^2 - \frac{c_2}{c_1} \right) \mathcal{G}_j \mathcal{S} + \mathcal{G}_j \left(\kappa - \frac{1}{c_1} \right) \mathcal{S}' + F_j \mathcal{S} \right) \sigma,$$

where

$$(51) \quad \tilde{f}_j = \mathcal{G}_j f_j - G_\Gamma^j(s, L) h_+ - G_\Gamma^j(s, 0) h_-.$$

As mentioned above, when enforcing the binormal boundary condition the operator \mathcal{S} does not map $H^2(\Gamma_*^j)$ to itself when Γ_*^j is an open curve. This issue is handled by an extension of the method of images described in the next subsection.

3.3. Mixed boundary conditions and a method of images approach. Before describing the image methods, we consider a provisional representation for the mixed-boundary problem on all of Γ . We introduce the notation $S_{*,i}$ for the layer potential S with density on Γ_*^i and $S_{\circ,i}$ for the layer potential S with density on Γ_\circ^i , and will use an analogous notation for D . We also let $\mathcal{S}_{\circ,j,*i}$ denote the restriction of the operator $S_{*,i}$ to Γ_\circ^j , and similarly for the other boundary components and operators, with $\mathcal{S}_{*,i} := \mathcal{S}_{*,i,*i}$, etc. used for the sake of brevity. For ease of exposition we consider the problem depicted in Figure 1b in which there are two pieces of the boundary with the visco-thermal boundary conditions (Γ_*^1, Γ_*^2) and two pieces with Robin boundary conditions $(\Gamma_\circ^1, \Gamma_\circ^2)$. Then, following the discussion above, we provisionally represent the solution as

$$(52) \quad u = \left(D_{*,1} - \frac{1}{c_1} S_{*,1} \right) \sigma_1 + \left(D_{*,2} - \frac{1}{c_1} S_{*,2} \right) \sigma_2 + S_{\circ,1} \rho_1 + S_{\circ,2} \rho_2.$$

The part of this representation acting from Γ_\circ^j to itself is

$$(53) \quad \frac{1}{2} \rho_j + a \mathcal{S}_{\circ,j} [\rho_j] + \mathcal{S}'_{\circ,j} [\rho_j],$$

which is Fredholm second kind.

It remains to check the singularity of the integral operators acting between Γ_* and Γ_\circ . The representation on Γ_*^i evaluated in the Robin boundary condition on Γ_\circ^j is given by

$$(54) \quad \left[a \left(\mathcal{D}_{\circ_j, *_i} - \frac{1}{c_1} \mathcal{S}_{\circ_j, *_i} \right) + \mathcal{D}'_{\circ_j, *_i} - \frac{1}{c_1} \mathcal{S}'_{\circ_j, *_i} \right] \sigma_i.$$

The most singular part of the operator above is $\mathcal{D}'_{\circ_j, *_i}$.

The representation on Γ_\circ^j evaluated in the visco-thermal boundary condition on Γ_*^i is

$$(55) \quad \left[c_1 (I + F_i) \mathcal{S}_{*, \circ_j} - \frac{1}{c_1} \mathcal{G}_i \mathcal{S}_{*, \circ_j} + \mathcal{G}_i \mathcal{S}'_{*, \circ_j} \right] \rho_j.$$

The most singular part of this integral operator is $F_i \mathcal{S}_{*, \circ_j}$.

To eliminate these singularities, we use an extension of the method of images. First, we treat the singularity of $\mathcal{D}'_{\circ_j, *_i}$ at the corner. For each boundary point $x_0 \in \partial\Gamma_*^i$, we consider the line ℓ spanned by the normal vector at that point. For some $R > 0$, we then define a curve via reflection of $\Gamma_*^i \cap B_R(x_0)$ across ℓ , which we call a *fin*. Next we define a modified double layer potential, $\tilde{D}_{*,i} \sigma_i$, which is obtained by extending the values of σ_i to the fins, with the values on the fin at each $x_0 \in \partial\Gamma_*^i$ defined by an even symmetric extension of the values of σ_i on $\Gamma_*^i \cap B_R(x_0)$, and evaluating the usual double layer induced by the extended density. An easy consequence of the even symmetry of the extended density, together with the symmetry of the extended domain and the additional assumptions on Γ_\circ (see Section 2.1), is that the kernel of the operator $\tilde{D}'_{\circ_j, *_i}$ is continuous away from the corner and bounded for source and target approaching the corner, and so the operator is compact (see Appendix B). We define $\tilde{\mathcal{S}}_{*,i}$ by even extension as well, which has the benefit that $\partial_s(\tilde{\mathcal{S}}_{*,i} \sigma_i)$ is defined at the endpoints.

Similarly, the singularity in $F_i \mathcal{S}_{*, \circ_j}$ can be eliminated by extending Γ_\circ^j by a fin and using an *odd* extension of ρ_j to define $\tilde{\mathcal{S}}_{\circ_j} \rho_j$. A proof of this fact is given in Appendix B. See Fig. 2 for a zoom-in of the fins near a corner.

Remark. While the image fins above are defined by reflection across the line parallel to the normal at the endpoint, it is useful in other settings to define them by other reflections or rotations. Similar fins were recently applied to regularize corner singularities that arose in a domain decomposition approach to waveguide problems [50]. The regularizing effect of including image curves with certain symmetries has also been observed in integral formulations of quasiperiodic scattering problems [51].

We now propose the fin-based representation

$$(56) \quad u = \left(\tilde{D}_{*1} - \frac{1}{c_1} \tilde{\mathcal{S}}_{*1} \right) \sigma_1 + \left(\tilde{D}_{*2} - \frac{1}{c_1} \tilde{\mathcal{S}}_{*2} \right) \sigma_2 + \tilde{\mathcal{S}}_{\circ 1} \rho_1 + \tilde{\mathcal{S}}_{\circ 2} \rho_2,$$

which utilizes even extensions for the Γ_*^i operators and odd extensions for the Γ_\circ^i operators. We make a substitution as in (49) and (50) so that the operator F_i is only applied to $\tilde{\mathcal{S}}_{*,i}$, outside of the enforcement of the binormal boundary condition. Define $\mathcal{K}_{*,i}$ to be the operator corresponding to the contribution of σ_i to the Γ_*^i boundary condition. After preconditioning as in Section 3.2.2, we have

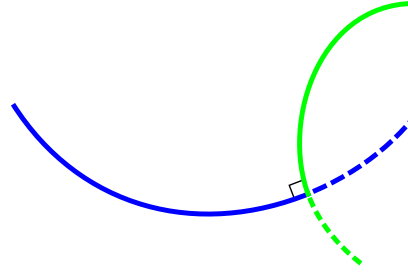


FIGURE 2. A zoom-in of the fins added to the geometry in the vicinity of a corner.

$$(57) \quad \mathcal{K}_{*,*,i} \sigma_i = \left(-\frac{c_1}{2} I_{*,i} + c_1 \tilde{\mathcal{D}}_{*,i} - \frac{1}{c_1} \mathcal{G}_i \tilde{\mathcal{D}}_{*,i} + \mathcal{G}_i (\tilde{\mathcal{D}}'_{*,i} + \tilde{\mathcal{S}}''_{*,i}) \right. \\ \left. + \left(k^2 - \frac{c_2}{c_1} \right) \mathcal{G}_i \tilde{\mathcal{S}}_{*,i} + \mathcal{G}_i \left(\kappa - \frac{1}{c_1} \right) \tilde{\mathcal{S}}'_{*,i} + F_i \tilde{\mathcal{S}}_{*,i} \right) \sigma_i$$

We define the operators of the remaining interactions analogously:

$$(58) \quad \mathcal{K}_{\circ_j,*,i} = a \left(\tilde{\mathcal{D}}_{\circ_j,*,i} - \frac{1}{c_1} \tilde{\mathcal{S}}_{\circ_j,*,i} \right) + \tilde{\mathcal{D}}'_{\circ_j,*,i} - \frac{1}{c_1} \tilde{\mathcal{S}}'_{\circ_j,*,i},$$

$$(59) \quad \mathcal{K}_{*,-,i} = c_1 \left(\tilde{\mathcal{D}}_{*,-,i} - \frac{1}{c_1} \tilde{\mathcal{S}}_{*,-,i} \right) - \frac{1}{c_1} \mathcal{G}_{-,i} \left(\tilde{\mathcal{D}}_{*,-,i} - \frac{1}{c_1} \tilde{\mathcal{S}}_{*,-,i} \right) \\ + \mathcal{G}_{-,i} \left(\tilde{\mathcal{D}}'_{*,-,i} - \frac{1}{c_1} \tilde{\mathcal{S}}'_{*,-,i} \right),$$

$$(60) \quad \mathcal{K}_{\circ_j,\circ_j} = \frac{1}{2} I_{\circ_j} + a \tilde{\mathcal{S}}_{\circ_j} + \tilde{\mathcal{S}}'_{\circ_j},$$

$$(61) \quad \mathcal{K}_{*,\circ_j} = c_1 \tilde{\mathcal{S}}_{*,\circ_j} - \frac{1}{c_1} \mathcal{G}_i \tilde{\mathcal{S}}_{*,\circ_j} + \mathcal{G}_i \tilde{\mathcal{S}}'_{*,\circ_j},$$

$$(62) \quad \mathcal{K}_{\circ_{-,j},\circ_j} = a \tilde{\mathcal{S}}_{\circ_{-,j},\circ_j} + \tilde{\mathcal{S}}'_{\circ_{-,j},\circ_j}.$$

Then, the full system is given by

$$(63) \quad \begin{bmatrix} \mathcal{K}_{*,1,*_1} & \mathcal{K}_{*,1,\circ_1} & \mathcal{K}_{*,1,*_2} & \mathcal{K}_{*,1,\circ_2} \\ \mathcal{K}_{\circ_1,1,*_1} & \mathcal{K}_{\circ_1,1,\circ_1} & \mathcal{K}_{\circ_1,1,*_2} & \mathcal{K}_{\circ_1,1,\circ_2} \\ \mathcal{K}_{*,2,*_1} & \mathcal{K}_{*,2,\circ_1} & \mathcal{K}_{*,2,*_2} & \mathcal{K}_{*,2,\circ_2} \\ \mathcal{K}_{\circ_2,2,*_1} & \mathcal{K}_{\circ_2,2,\circ_1} & \mathcal{K}_{\circ_2,2,*_2} & \mathcal{K}_{\circ_2,2,\circ_2} \end{bmatrix} \begin{bmatrix} \sigma_1 \\ \rho_1 \\ \sigma_2 \\ \rho_2 \end{bmatrix} = \begin{bmatrix} \tilde{f}_1 \\ g_1 \\ \tilde{f}_2 \\ g_2 \end{bmatrix},$$

where the modified data \tilde{f}_1, \tilde{f}_2 are defined as in (51). Denote the operator in (63) by \mathcal{M} . The following theorem states that, up to a bounded operator with bounded inverse, \mathcal{M} is Fredholm second-kind.

Theorem 3.4. *The operator $\mathcal{M} : H^2(\Gamma_*) \times L^2(\Gamma_\circ) \rightarrow H^2(\Gamma_*) \times L^2(\Gamma_\circ)$ is of the form $A + K$, where K is compact and A is boundedly invertible.*

Proof. The diagonal operators $\mathcal{K}_{*,*,i}$ and $\mathcal{K}_{\circ_j,\circ_j}$ are Fredholm second-kind, and the off-diagonal operators $\mathcal{K}_{*,-,i}$ and $\mathcal{K}_{\circ_{-,j},\circ_j}$ are compact, on their respective spaces. The operators

$$(64) \quad \tilde{\mathcal{S}}'_{*,i} : L^2(\Gamma_\circ^j) \rightarrow L^2(\Gamma_*^i),$$

$$(65) \quad \tilde{\mathcal{D}}_{\circ_j, *_i} : L^2(\Gamma_*^i) \rightarrow L^2(\Gamma_\circ^j)$$

are bounded [45]. The operator

$$(66) \quad \mathcal{G}_i : L^2(\Gamma_*^i) \rightarrow H^2(\Gamma_*^i)$$

is also bounded, so the composition

$$(67) \quad \mathcal{G}_i \tilde{\mathcal{S}}'_{*,i,\circ_j} : L^2(\Gamma_\circ^j) \rightarrow H^2(\Gamma_*^i)$$

is bounded. The odd-symmetric fins on Γ_\circ^j render

$$(68) \quad \tilde{\mathcal{S}}_{*,i,\circ_j} : L^2(\Gamma_\circ^j) \rightarrow H^2(\Gamma_*^i)$$

compact, and thus $\mathcal{K}_{*,i,\circ_j}$ is bounded. Since the inclusion

$$(69) \quad H^2(\Gamma_*^i) \hookrightarrow L^2(\Gamma_*^i)$$

is compact ([48, 49]) and (65) is bounded, the composition

$$(70) \quad \tilde{\mathcal{D}}_{\circ_j, *_i} : H^2(\Gamma_*^i) \rightarrow L^2(\Gamma_\circ^j)$$

is compact, and thus so too is $\mathcal{K}_{\circ_j, *_i}$.

Collect the compact operators in a 4x4 matrix of operators, denoted K , and let $A = 2(\mathcal{M} - K)$. Then

$$(71) \quad A = \begin{bmatrix} -c_1 I_{*,1,*_1} & A_{11} & & A_{12} \\ & I_{\circ_1,\circ_1} & & \\ & A_{21} & -c_1 I_{*,2,*_2} & A_{22} \\ & & I_{\circ_2,\circ_2} & \end{bmatrix},$$

where the operators $A_{ij} : L^2(\Gamma_\circ^j) \rightarrow H^2(\Gamma_*^i)$ are bounded. We then have

$$(72) \quad \Pi^\top A \Pi = \begin{bmatrix} -c_1 I_{*,1,*_1} & A_{11} & A_{12} & \\ & -c_1 I_{*,2,*_2} & A_{21} & A_{22} \\ & & I_{\circ_1,\circ_1} & \\ & & I_{\circ_2,\circ_2} & \end{bmatrix},$$

where Π is a block permutation. The inverse of this operator is obtained by negating the strictly upper triangular part and multiplying by the appropriate diagonal matrix. \square

At this point it is worth noting the following special case. Suppose that f and h are identically zero, as is the case in many problems of interest. In this case, using Schur complements, we reduce (63) to a second-kind integral equation solely on Γ_\circ . Let

$$(73) \quad \mathcal{K}_{*,\circ} = [\mathcal{K}_{*,\circ_1} \quad \mathcal{K}_{*,\circ_2}],$$

$$(74) \quad \mathcal{K}_{\circ_i,*} = [\mathcal{K}_{\circ_i,*_1} \quad \mathcal{K}_{\circ_i,*_2}],$$

$$(75) \quad \mathcal{K}_{\circ,*_i} = \begin{bmatrix} \mathcal{K}_{\circ_1,*_i} \\ \mathcal{K}_{\circ_2,*_i} \end{bmatrix},$$

$$(76) \quad \mathcal{K}_{*,\circ_i} = \begin{bmatrix} \mathcal{K}_{*,\circ_1} \\ \mathcal{K}_{*,\circ_2} \end{bmatrix},$$

$$(77) \quad \mathcal{K}_\circ = \begin{bmatrix} \mathcal{K}_{\circ_1,\circ_1} & \mathcal{K}_{\circ_1,\circ_2} \\ \mathcal{K}_{\circ_2,\circ_1} & \mathcal{K}_{\circ_2,\circ_2} \end{bmatrix}.$$

Assuming that $\mathcal{K}_{*,*i}$ is invertible, we define

$$(78) \quad \mathcal{A}_i = \mathcal{K}_{*-i,*i} \mathcal{K}_{*,*i}^{-1},$$

Since $\mathcal{K}_{*-i,*i}$ is compact, $\mathcal{K}_{*,*i} - \mathcal{A}_{-i} \mathcal{K}_{*-i,*i}$ is also Fredholm second-kind. Suppose that it is invertible as well. We then define the operator

$$(79) \quad \mathcal{B}_i = (\mathcal{K}_{*,*i} - \mathcal{A}_{-i} \mathcal{K}_{*-i,*i})^{-1} (\mathcal{A}_{-i} \mathcal{K}_{*-i,o} - \mathcal{K}_{*,o}).$$

By taking Schur complements, (63) is equivalent to solving the reduced system

$$(80) \quad (\mathcal{K}_o + \mathcal{K}_{o,*i} \mathcal{B}_1 + \mathcal{K}_{o,*2} \mathcal{B}_2) \rho = g.$$

Note that $\mathcal{B}_i : \rho \mapsto \sigma_i$. Let the operator in (80) be denoted by $\mathcal{M}_{o,r}$.

Corollary 3.4.1. $\mathcal{M}_{o,r} : L^2(\Gamma_o) \rightarrow L^2(\Gamma_o)$ is Fredholm second-kind.

Proof. In the proof of Theorem 3.4, it was already shown that $\mathcal{K}_{*,o}$ is bounded and $\mathcal{K}_{o,*i}$ is compact. Hence \mathcal{B}_i is bounded, and the composition $\mathcal{K}_{o,*i} \mathcal{B}_i$ is compact. Since \mathcal{K}_o is Fredholm second-kind, the statement follows. \square

3.4. Domain decomposition and impedance-to-impedance. For complicated domains with multiscale features or modular components, it is often advantageous to divide the domain into multiple regions. Given a solver for each individual region, there are several methods of coupling them together, thus obtaining a solution to the full problem. Here, we briefly outline the use of impedance-to-impedance maps (see, e.g., [52]) to enforce continuity of the solution and its normal derivative across each artificial boundary.

In the previous analysis, the solution u for Case II is assumed to satisfy a general Robin boundary condition on the portion of the boundary denoted by Γ_o , see (4). As special cases, the solution is said to satisfy an incoming impedance condition if

$$(81) \quad iku + \partial_n u = g,$$

and an outgoing impedance condition if

$$(82) \quad -iku + \partial_n u = g.$$

Let \mathcal{M}^+ (resp. \mathcal{M}^-) denote the operator in (63) with $a = ik$ (resp. $a = -ik$). Similarly define $\mathcal{M}_{o,r}^\pm$ for the reduced version of \mathcal{M}^\pm , given in (80). Then the impedance-to-impedance maps are given by

$$(83) \quad \mathcal{I}_{-,+} = \mathcal{M}_{o,r}^-(\mathcal{M}_{o,r}^+)^{-1},$$

$$(84) \quad \mathcal{I}_{+,-} = \mathcal{M}_{o,r}^+(\mathcal{M}_{o,r}^-)^{-1},$$

provided that each of $\mathcal{M}_{o,r}^\pm$ are invertible. Since invertible Fredholm second-kind operators form a group under composition, the impedance-to-impedance maps are Fredholm second-kind operators when they are defined. Once one has access to the impedance-to-impedance maps, by matching incoming and outgoing impedance data on each side of Γ_o , continuity of the solution and its normal derivative is enforced.

Remark. Although the impedance-to-impedance maps are Fredholm second-kind, the system obtained by imposing continuity of the incoming and outgoing impedance data has a degeneracy in the identity part, making it only compact. However, empirically, we observe that the condition number of the system does not exceed 10^4 for our discretizations.

4. NUMERICS

In the figures below, as representative values we take boundary layer thicknesses $\delta_V = \delta_T = \frac{1}{160}$, specific heat ratio $\gamma = 1.4$, and wavelength $\lambda = 1.1$.

For our simulations we use the chunkIE software package [53]. The package discretizes the boundary of a domain via curved panels of Gauss-Legendre nodes. We use 16th order panels in the calculations below, and the panel lengths are selected to be less than $\lambda/4$. Additionally, for geometries with corners, we use dyadically refined panels near the corner points, to a depth of seven levels. For well-separated panels, the classical Gauss-Legendre quadrature is used. For adjacent panels and for the interaction of a panel with itself, adaptive integration and generalized Gauss-Legendre quadratures are used, see [54, 55]. The package also implements a surface smoother ([56]) which we use for the generation of our example for Case I.

The geometry we use to illustrate Case I consists of a waveguide spiraling outward from a circular cavity. We consider the solution due to a point source located at $(x, y) = (-0.4, 0.3)$. The absolute value of the solution is shown in figure 3.

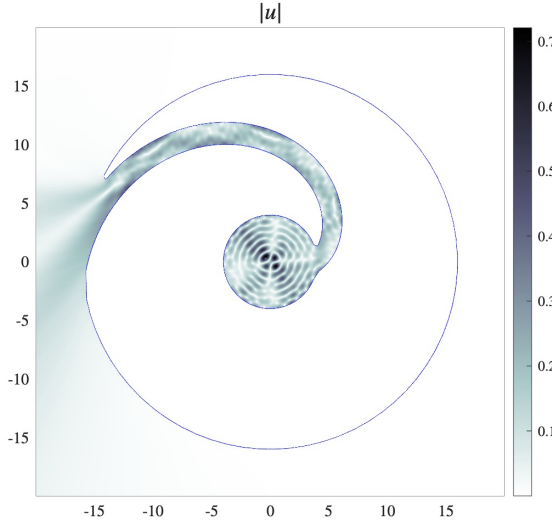


FIGURE 3. Magnitude of the solution due to a point source at $(x, y) = (-0.4, 0.3)$, for the geometry outlined in blue.

Our first example for Case II is a solution to (4), where the domain Ω is taken to be a curved waveguide of finite length. The geometry is shown in figure 4. On the boundary Γ_* we take $f = 0$, and on $\partial\Gamma_*$, $h = 0$. Let Γ_0^1 denote the left boundary, and let Γ_0^2 denote the right boundary. Take $g \equiv 0$ on Γ_0^2 , and on Γ_0^1 take g to be the incoming impedance (see (81)) due to a point source at $(x, y) = (-16.1, 0)$. This is a rough approximation to the solution due to a point source at that location. The real part of the solution is given in figure 5. This geometry passes the analytic solution test to $\sim 10^{-7}$.

Next we consider the solution due purely to an inhomogeneity in the binormal boundary condition, imposed on the bottom left and top left corners of a curved

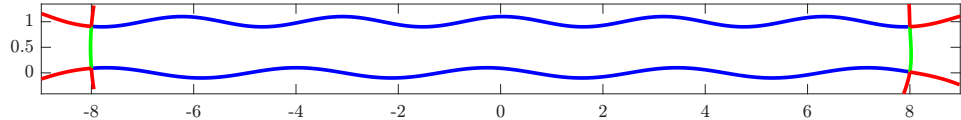


FIGURE 4. On the boundary of the waveguide, visco-thermal boundary conditions are used (blue), while the caps of the waveguide are given a Robin boundary condition (green). Artificial fins extend off of the corners into the exterior of the domain (red).

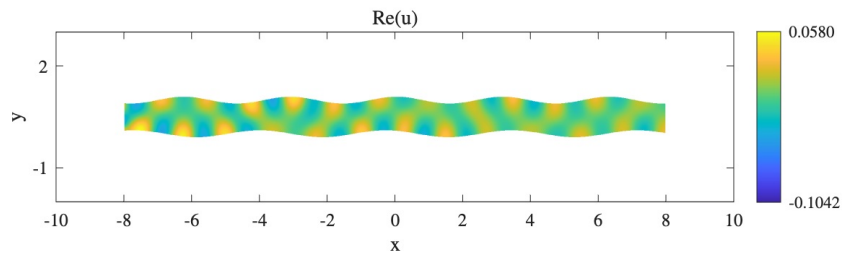


FIGURE 5. Real part of the solution with incoming impedance on the left boundary due to a point source.

waveguide. The binormal data is due to point sources at $(x, y) = (-8.1, 0)$ and $(x, y) = (-8.1, 0.9)$. The real part of the solution is shown in figure 6.

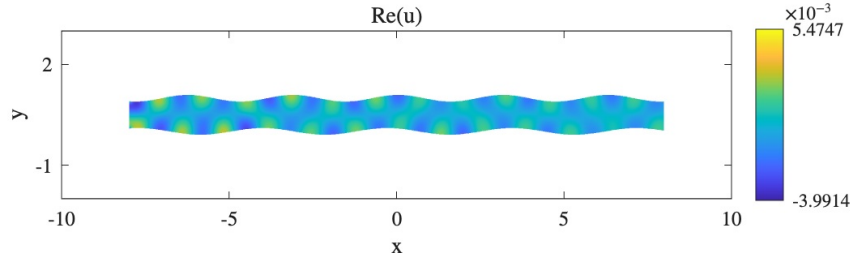


FIGURE 6. Real part of the solution with binormal data due to point sources near the two leftmost corners.

In our third example for Case II, we employ impedance-to-impedance maps to decompose a complicated domain into smaller pieces (see 3.4). The geometry is shown in figure 7. There are three waveguides with curved boundary, each connecting the triangular region on the inside to the exterior of a larger triangle. Visco-thermal boundary conditions are imposed on the boundary of the waveguide, while Neumann boundary conditions are imposed on the boundary of the triangles. The absolute value of the solution is shown in Figure 8. The analytic solution test for this problem is correct to $\sim 10^{-7}$.

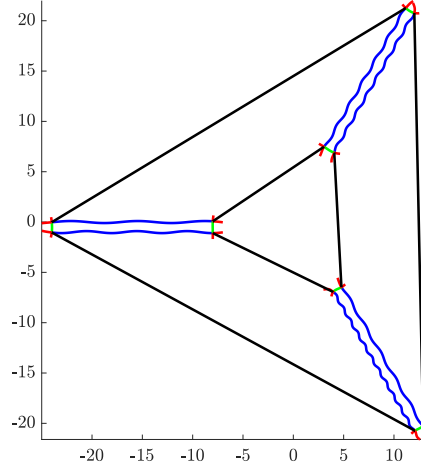


FIGURE 7. On the physical boundary, either Neumann (black) or visco-thermal (blue) boundary conditions are imposed. The artificial boundary, where the impedance-to-impedance matching is performed, is denoted in green. The artificial fins used for canceling corner singularities are denoted in red.

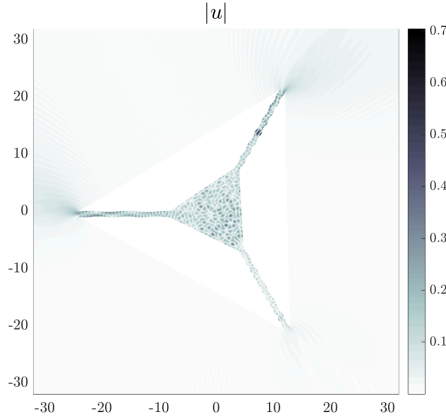


FIGURE 8. Magnitude of the solution due to a point source $(x, y) = (0.5, 0.6)$, solved using domain decomposition.

Our final example for Case II uses a geometry inspired by the cross-section of a ‘phase plug’. The geometry is shown in Figure 9, where the different sections of the physical and artificial boundaries are denoted as in Figure 7. The condition $\partial_n u = 1$ is imposed on the rear wall of the interior of the geometry. All other boundary conditions are homogeneous. The absolute value of the solution is shown in Figure 10. The analytic solution test for this problem is correct to $\sim 10^{-7}$.

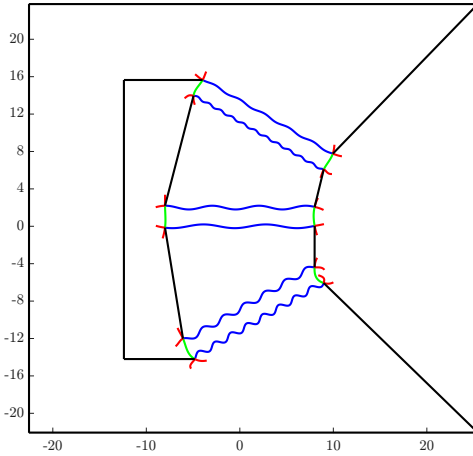


FIGURE 9. A geometry inspired by the cross-section of a phase plug. On the physical boundary, Neumann and viscothermal boundary conditions are imposed on the black and blue boundaries, respectively. The artificial boundary used for impedance-to-impedance matching is denoted in green, and the fins are denoted in red.

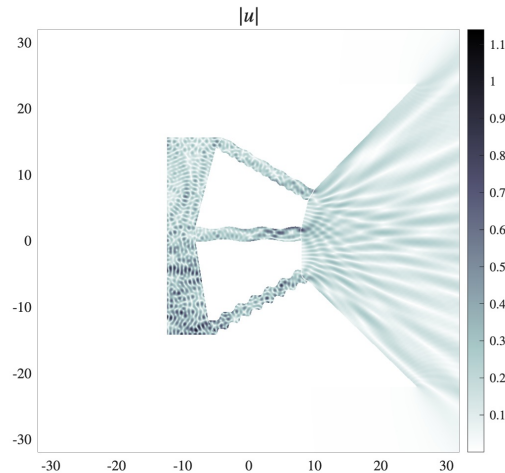


FIGURE 10. Magnitude of the solution due to the inhomogeneity $\partial_n u = 1$ on the back wall of the interior of the device, solved using domain decomposition.

5. CONCLUSION

A novel integral representation for the solution of the Helmholtz equation with visco-thermal boundary conditions is proposed. Two cases are considered: a smooth boundary where visco-thermal boundary conditions are imposed, and a piecewise

smooth boundary with mixed boundary conditions. In the latter case, the impedance-to-impedance map is used to link the solution in an acoustically narrow region to a solution in a larger region. In the first case, the integral equation we obtain is Fredholm second-kind, while in the second case, it is Fredholm second-kind up to a boundedly invertible operator. In forthcoming work, the authors will develop an integral formulation for the three dimensional version of this problem.

ACKNOWLEDGMENT

J.G.H. was supported in part by a Sloan Research Fellowship. This research was supported in part by grants from the NSF (DMS-2235451) and Simons Foundation (MPS-NITMB-00005320) to the NSF-Simons National Institute for Theory and Mathematics in Biology (NITMB). The authors thank Alex Barnett for suggesting this problem and Manas Rachh for many useful discussions.

APPENDIX A.

Proof of Lemma 3.2. The kernel of \mathcal{D} on surface is of the form $\mu(s) + s^2 \log(s)\nu(s)$, where μ and ν are smooth, so by the dominated convergence theorem, the kernel of Δ_Γ applied to \mathcal{D} on surface is $\Delta_\Gamma \partial_{n_y} G$. Since the Laplace-Beltrami operator is the second arclength derivative, this implies $\Delta_\Gamma \partial_{n_y} G$ is at most logarithmically singular.

It is worth noting that since the kernel of D satisfies the Helmholtz equation whenever $x \neq y$, (21) implies that *on surface*,

$$(85) \quad \Delta_\Gamma \mathcal{D} \sigma = -k^2 \mathcal{D} \sigma - (\kappa \mathcal{D}' + \mathcal{D}'') \sigma,$$

and that $\kappa \mathcal{D}' + \mathcal{D}''$ has logarithmically singular kernel.

Now consider the limiting quantity for some finite h . Since $D\sigma$ satisfies the Helmholtz equation away from Γ , we have

$$(86) \quad \Delta_\Gamma \mathcal{D}_{\Gamma_h, \Gamma} \sigma = -k^2 \mathcal{D}_{\Gamma_h, \Gamma} \sigma - \kappa_h \mathcal{D}'_{\Gamma_h, \Gamma} \sigma - \mathcal{D}''_{\Gamma_h, \Gamma} \sigma,$$

where κ_h denotes the curvature on Γ_h . The jump of D is given by (12), and D' is continuous in the sense of (15). It remains to compute the jump of D'' .

Let $\vec{r} = x - y$ and $r = |\vec{r}|$. As $r \rightarrow 0$, the Green's function satisfies the expansion

$$(87) \quad \frac{i}{4} H_0^{(1)}(kr) = -\frac{1}{2\pi} \log(r) + \frac{k^2}{8\pi} r^2 \log(r) + \mathcal{O}(r^4 \log(r)).$$

Let D_0 denote the Laplace double layer operator, and define

$$(88) \quad T[\sigma](x) = \int_\Gamma [\partial_{n_y} r^2 \log(r)] \sigma(y) \, ds(y).$$

Then (87) implies that

$$(89) \quad \mathcal{D}_{\Gamma \rightarrow \Gamma_h}'' = (\mathcal{D}_0'')_{\Gamma_h, \Gamma} + \frac{k^2}{8\pi} T_{\Gamma_h, \Gamma}'' + M,$$

where M is continuous across Γ . The following limit is derived in [43]:

$$(90) \quad \lim_{h \rightarrow 0} (\mathcal{D}_0'')_{\Gamma_h, \Gamma} \sigma = \frac{1}{2} \Delta_\Gamma \sigma + \mathcal{D}_0'' \sigma.$$

It remains to compute the jump of T'' . Let $\gamma : (0, L) \rightarrow \mathbb{R}^2$ be an arc-length parameterization of Γ , and fix $y_0 = \gamma(s_0)$. Take $x = y_0 - hn_{y_0}$ and $y = \gamma(s_0 + s)$. Then, by Taylor's theorem,

$$(91) \quad \partial_{n_x}^2 \partial_{n_y} r^2 \log(r) = \frac{2h^3 + 6hs^2}{(h^2 + s^2)^2} + \zeta(h, s),$$

where $\zeta = \mathcal{O}(1)$. Define $\Gamma^\epsilon = \gamma([0, s_0 - \epsilon]) \cup \gamma([s_0 + \epsilon, L])$. Then

$$(92) \quad \begin{aligned} T''[\sigma](x) &= \int_{-\epsilon}^{\epsilon} \frac{2h^3 + 6hs^2}{(h^2 + s^2)^2} \sigma(y(s)) \, ds \\ &\quad + \int_{-\epsilon}^{\epsilon} \zeta(h, s) \sigma(y(s)) \, ds \\ &\quad + \int_{\Gamma^\epsilon} [\partial_{n_x}^2 \partial_{n_y} r^2 \log(r)] \sigma(y) \, ds(y). \end{aligned}$$

The latter two integrals have no jump as $h \rightarrow 0$. For the former we compute

$$(93) \quad \begin{aligned} \int_{-\epsilon}^{\epsilon} \frac{2h^3 + 6hs^2}{(h^2 + s^2)^2} \sigma(y(s)) \, ds &= \sigma(y_0) \int_{-\epsilon}^{\epsilon} \frac{2h^3 + 6hs^2}{(h^2 + s^2)^2} \, ds \\ &\quad + \int_{-\epsilon}^{\epsilon} \frac{2h^3 + 6hs^2}{(h^2 + s^2)^2} [\sigma(y(s)) - \sigma(y_0)] \, ds. \end{aligned}$$

For $\sigma \in C^1(\Gamma)$, we have $\sigma(y(s)) - \sigma(y_0) = \mathcal{O}(s)$. Since $C^1(\Gamma) \supset H^2(\Gamma)$ ([48]) the latter integrand is bounded as $h \rightarrow 0$, and its integral vanishes in the limit $\epsilon \rightarrow 0$. The former integral is evaluated in the limit $h \rightarrow 0$ as

$$(94) \quad \begin{aligned} \sigma(y_0) \int_{-\epsilon}^{\epsilon} \frac{2h^3 + 6hs^2}{(h^2 + s^2)^2} \, ds &= \sigma(y_0) \left[8 \arctan\left(\frac{\epsilon}{h}\right) - 4 \frac{h\epsilon}{h^2 + \epsilon^2} \right] \\ &\rightarrow 4\pi\sigma(y_0). \end{aligned}$$

This implies that

$$(95) \quad \lim_{h \rightarrow 0} T''_{\Gamma \rightarrow \Gamma_h} \sigma = 4\pi\sigma + T''\sigma,$$

and thus, the limit of (89) is

$$(96) \quad \lim_{h \rightarrow 0} \mathcal{D}''_{\Gamma \rightarrow \Gamma_h} \sigma = \frac{1}{2} \Delta_\Gamma \sigma + \frac{k^2}{2} \sigma + \mathcal{D}''\sigma.$$

To summarize, the limit of (86) is

$$(97) \quad \begin{aligned} \lim_{h \rightarrow 0} \Delta_\Gamma \mathcal{D}_{\Gamma \rightarrow \Gamma_h} \sigma &= -k^2 \left(-\frac{I}{2} + \mathcal{D} \right) \sigma - \kappa \mathcal{D}' \sigma - \left(\frac{1}{2} \Delta_\Gamma + \frac{k^2}{2} I + \mathcal{D}'' \right) \sigma \\ &= -\frac{1}{2} \Delta_\Gamma \sigma - k^2 \mathcal{D} \sigma - (\kappa \mathcal{D}' + \mathcal{D}'') \sigma. \end{aligned}$$

□

Remark. We note that the limit we derive in (96) differs from that derived in [43] by a factor of 4 in the identity term.

APPENDIX B.

In this section we give proof of the regularizing effect of the addition of fins to the corners in our representation described in section 3.3. Recall from section 2.1 that the curves Γ_*^i and Γ_\circ^j are assumed to meet orthogonally at each corner. Throughout, we will let s denote the arc length along Γ_*^i from the corner of interest, and t denote the arc length along Γ_\circ^j from the same corner.

We let $x(s)$ be the arclength parameterization of Γ_*^i starting at the corner, and let $y(t)$ be the arclength parameterization of Γ_\circ^j . Denote the normal vector at $x(s)$ by $n_x(s)$, the normal vector at $y(t)$ by $n_y(t)$, and analogously for the tangent vector τ and curvature κ . We assume without loss of generality that $\tau_y(0) = -n_x(0)$.

In this case, Taylor's theorem gives the following expansions on Γ_*^i :

$$(98) \quad x(s) = -\tau_x(0)s - \frac{1}{2}\kappa_x(0)n_x(0)s^2 + \mathcal{O}(s^3),$$

$$(99) \quad n_x(s) = n_x(0) - \kappa_x(0)\tau_x(0)s + \mathcal{O}(s^2).$$

Reflecting Γ_*^i across the line spanned by $n_x(0)$ therefore corresponds, up to $\mathcal{O}(s^3)$ in x and $\mathcal{O}(s^2)$ in n_x , to the map $s \mapsto -s$. An analogous statement holds for Γ_\circ^j . It will thus suffice in the computations below to consider the even and odd parts of the kernels of interest, in s and t separately, as appropriate.

Consider first the kernel of $\mathcal{D}'_{\circ_j, *_i}$ in the vicinity of the corner. Due to the expansion (87), it in fact suffices to consider the kernel of the corresponding Laplace operator $(\mathcal{D}'_0)_{\circ_j, *_i}$. We write this in terms of s and t as

$$(100) \quad \begin{aligned} -\frac{1}{2\pi} \partial_{n_x n_y} \log r &= \frac{1}{2\pi} \left(\frac{n_x \cdot n_y}{r^2} - 2 \frac{(n_x \cdot \vec{r})(n_y \cdot \vec{r})}{r^4} \right) \\ &= \frac{1}{2\pi} \frac{1}{(s^2 + t^2)^3} (2ts^3 + 2t^3s - \kappa_y(0)ts^4 + 3\kappa_x(0)t^2s^3 \\ &\quad + 3\kappa_y(0)t^3s^2 - \kappa_x(0)t^4s + \mathcal{O}((s^2 + t^2)^3)). \end{aligned}$$

Up to bounded terms, the effective kernel of the operator $(\tilde{\mathcal{D}}'_0)_{\circ_j, *_i}$, modified by the addition of even-symmetric fins, is twice the even part of the above, in s :

$$(101) \quad \frac{1}{\pi} \frac{1}{(s^2 + t^2)^3} \kappa_y(0) (-ts^4 + 3t^3s^2) + \mathcal{O}(1).$$

Since $\kappa_y(0) = 0$ by assumption (see section 2.1), this implies that the kernel of $\tilde{\mathcal{D}}'_{\circ_j, *_i}$ is bounded in the vicinity of the corner. Hence the operator $\tilde{\mathcal{D}}'_{\circ_j, *_i}$ is compact from $H^2(\Gamma_*^i)$ to $L^2(\Gamma_\circ^j)$.

The singular part of $F_i \mathcal{S}_{*, \circ_j}$ arises from the evaluation of $\partial_\tau \mathcal{S}_{*, \circ_j}$ at the corner. Again it suffices to consider the Laplace kernel: this is computed as

$$(102) \quad \begin{aligned} -\frac{1}{2\pi} \partial_{\tau_x} \log r &= -\frac{\tau_x \cdot \vec{r}}{r^2} \\ &= \frac{s + \mathcal{O}(s^2 + t^2)}{s^2 + t^2}. \end{aligned}$$

Up to bounded terms, the effective kernel of the operator $\partial_\tau \tilde{\mathcal{S}}_{*, \circ_j}$, modified by the addition of odd-symmetric fins, is twice the odd part of the above, in t . Thus its kernel is bounded in the vicinity of the corner, as desired.

REFERENCES

- [1] W.R. Kampinga. *Viscothermal acoustics using finite elements*. phdthesis, University of Twente, 2010.
- [2] Júlio A. Cordioli, Gustavo Martins, and Roberto Jordan. A comparison of visco-thermal models for the vibro-acoustic analysis of hearing aids. *The Journal of the Acoustical Society of America*, 127(3):1770–1770, 2010.
- [3] D. Homentcovschi, R. N. Miles, P. V. Loeppert, and A. J. Zuckerwar. A microacoustic analysis including viscosity and thermal conductivity to model the effect of the protective cap on the acoustic response of a MEMS microphone. *Microsystem Technologies*, 20(2):265–272, 2014.
- [4] Vahid Naderyan, Richard Raspet, Craig Hickey, and Mohammad Mohammadi. Computational viscothermal acoustic study of micro-electro-mechanical systems (MEMS) perforated plates. *The Journal of the Acoustical Society of America*, 145(3):1863–1863, 2019.
- [5] Hamideh Hassanpour Guilvaei, Florian Toth, and Manfred Kaltenbacher. FEM-modeling of thermal and viscous effects in piezoelectric MEMS loudspeakers. *PAMM*, 22(1):e202200027, 2023.
- [6] Vicente Cutanda Henríquez, Victor M. García-Chocano, and José Sánchez-Dehesa. Viscothermal losses in double-negative acoustic metamaterials. *Physical Review Applied*, 8(1):014029, 2017.
- [7] Miguel Molerón, Marc Serra-Garcia, and Chiara Daraio. Visco-thermal effects in acoustic metamaterials: from total transmission to total reflection and high absorption. *New Journal of Physics*, 18(3):033003, 2016.
- [8] José Sánchez-Dehesa and Vicente Cutanda Henríquez. Visco-thermal effects in acoustic metamaterials based on local resonances. In Vicente Romero-García and Anne-Christine Hladky-Hennion, editors, *Fundamentals and Applications of Acoustic Metamaterials*, pages 1–24. Wiley, 1 edition, 2019.
- [9] Mora Joseph, Vroumsia David, Mibaile Justin, Sylvère Sindanne Azakine, Gambo Betchewe, and Doka Yamigno Serge. Impact of viscothermal loss on modulation instability and rogue waves in left-handed nonlinear diffractive acoustic transmission line metamaterials. *Physica Scripta*, 99(2):025213, 2024.
- [10] Jesús Carbajo, Jaime Ramis, Luís Godinho, Paulo Amado-Mendes, and Jesús Alba. A finite element model of perforated panel absorbers including viscothermal effects. *Applied Acoustics*, 90:1–8, 2015.
- [11] R. Billard, G. Tissot, G. Gabard, and M. Versaevel. Numerical simulations of perforated plate liners: Analysis of the visco-thermal dissipation mechanisms. *The Journal of the Acoustical Society of America*, 149(1):16–27, 2021.
- [12] Wei Na and Huadong Yao. A unified approach coupling linearized navier-stokes equations and helmholtz equations to predict sound propagation with viscothermal losses in acoustic liners, 2023.
- [13] Martin Berggren, Daniel Noreland, and Anders Bernland. A highly efficient approach to model acoustics with visco-thermal boundary losses. *The Journal of the Acoustical Society of America*, 144(3):1792–1792, 2018.
- [14] Peter Risby Andersen, Vicente Cutanda Henríquez, and Niels Aage. Shape optimization of micro-acoustic devices including viscous and thermal losses. *Journal of Sound and Vibration*, 447:120–136, 2019.
- [15] René Christensen and Ulrik Skov. Compression driver simulation incl. vibroacoustic, viscothermal & porous acoustics. In *COMSOL Conference in Stuttgart*. COMSOL, 2011.
- [16] Anders Bernland, Eddie Wadbro, and Martin Berggren. Shape optimization of a compression driver phase plug. *SIAM Journal on Scientific Computing*, 41(1):B181–B204, 2019. Publisher: Society for Industrial & Applied Mathematics (SIAM).
- [17] Martin Berggren, Anders Bernland, André Massing, Daniel Noreland, and Eddie Wadbro. A better compression driver? CutFEM 3d shape optimization taking viscothermal losses into account, 2024.
- [18] Abbas Mousavi, Martin Berggren, and Eddie Wadbro. Extending material distribution topology optimization to boundary-effect-dominated problems with applications in viscothermal acoustics. *Materials & Design*, 234:112302, 2023. Publisher: Elsevier BV.

- [19] Yuki Noguchi and Takayuki Yamada. Topology optimization for acoustic structures considering viscous and thermal boundary layers using a sequential linearized navier-stokes model. *Computer Methods in Applied Mechanics and Engineering*, 394:114863, 2022.
- [20] Sumer B. Dilgen, Niels Aage, and Jakob S. Jensen. Three dimensional vibroacoustic topology optimization of hearing instruments using cut elements. *Journal of Sound and Vibration*, 532:116984, 2022. Publisher: Elsevier BV.
- [21] Gilles Tissot, Robin Billard, and Gwénaël Gabard. Optimal cavity shape design for acoustic liners using helmholtz equation with visco-thermal losses. *Journal of Computational Physics*, 402:109048, 2020. Publisher: Elsevier BV.
- [22] V. Cutanda Henríquez and P. Risby Andersen. A three-dimensional acoustic boundary element method formulation with viscous and thermal losses based on shape function derivatives. *Journal of Theoretical and Computational Acoustics*, 26(3):1850039, 2018.
- [23] C Sambuc, G Lielens, and Jean-Pierre Coyette. Numerical modelling of visco-thermal acoustics using finite elements. In *ISMA*, 2014.
- [24] W. R. Kampinga, Y. H. Wijnant, and A. De Boer. Performance of several viscothermal acoustic finite elements. *Acta Acustica united with Acustica*, 96(1):115–124, 2010.
- [25] Mark J. Cops, J. Gregory McDaniel, Elizabeth A. Magliula, David J. Bamford, and Martin Berggren. Estimation of acoustic absorption in porous materials based on visco-thermal boundary layers modeled as boundary conditions. *The Journal of the Acoustical Society of America*, 148(3):1624–1635, 2020.
- [26] Simone Preuss, Mikkel Paltorp, Alexis Blanc, Vicente Cutanda Henríquez, and Steffen Marburg. Revising the boundary element method for thermoviscous acoustics: An iterative approach via schur complement. *Journal of Theoretical and Computational Acoustics*, 31(4):2350015, 2023.
- [27] M. Paltorp and V. Cutanda Henríquez. An open-source boundary element framework for large-scale viscothermal acoustics. In *Proceedings of the 10th Convention of the European Acoustics Association Forum Acusticum 2023*, pages 5651–5658. European Acoustics Association, 2024.
- [28] Peter Risby Andersen. *Modelling of acoustic viscothermal losses using the Boundary Element Method: From method to optimization*. phdthesis, Technical University of Denmark, 2018.
- [29] Martin Berggren, Anders Bernland, and Daniel Noreland. Acoustic boundary layers as boundary conditions. *Journal of Computational Physics*, 371:633–650, 2018.
- [30] B Aslanyürek, Houssem Haddar, and H Şahintürk. Generalized impedance boundary conditions for thin dielectric coatings with variable thickness. *Wave Motion*, 48(7):681–700, 2011.
- [31] Xavier Antoine, Hélène Barucq, and Laurent Vernhet. High-frequency asymptotic analysis of a dissipative transmission problem resulting in generalized impedance boundary conditions. *Asymptotic Analysis*, 26(3-4):257–283, 2001.
- [32] Habib Ammari and J-C Nédélec. Generalized impedance boundary conditions for the maxwell equations as singular perturbations problems. *Communications in partial differential equations*, 24(5-6):24–38, 1999.
- [33] John D Shumpert and Thomas BA Senior. Impedance boundary conditions in ultrasonics. *IEEE Transactions on Antennas and Propagation*, 48(10):1653–1659, 2000.
- [34] Fioralba Cakoni and Rainer Kress. Integral equation methods for the inverse obstacle problem with generalized impedance boundary condition. *Inverse Problems*, 29(1):015005, 2012.
- [35] A. D. Venttsel'. On boundary conditions for multidimensional diffusion processes. *Theory of Probability & Its Applications*, 4(2):164–177, 1959. Publisher: Society for Industrial & Applied Mathematics (SIAM).
- [36] Giuseppe M Coclite, Angelo Favini, Ciprian G Gal, Ruiz Goldstein, Jerome A Goldstein, Enrico Obrecht, and Silvia Romanelli. The role of wentzell boundary conditions in linear and nonlinear analysis. *Tübinger Berichte zur Funktionalanalysis*, 16:132–144, 2007/2008. Arbeitsgemeinschaft Funktionalanalysis (AGFA), University of Tübingen.
- [37] Kendall E. Atkinson. *The numerical solution of integral equations of the second kind*. Cambridge monographs on applied and computational mathematics; 4; 4. Cambridge University Press, Cambridge, 1997.
- [38] L. Greengard, Jingfang Huang, V. Rokhlin, and S. Wandzura. Accelerating fast multipole methods for the helmholtz equation at low frequencies. *IEEE Computational Science and Engineering*, 5(3):32–38, 1998.

- [39] Stefan A Sauter and Christoph Schwab. Boundary element methods. *Springer Series in Computational Mathematics*, 2011.
- [40] David Colton and Rainer Kress. *Integral equation methods in scattering theory*. Number 72 in Classics in applied mathematics. SIAM, 2013.
- [41] Per-Gunnar Martinsson. *Fast direct solvers for elliptic PDEs*. SIAM, 2019.
- [42] NIST Digital Library of Mathematical Functions. <https://dlmf.nist.gov/>, Release 1.2.4 of 2025-03-15. F. W. J. Olver, A. B. Olde Daalhuis, D. W. Lozier, B. I. Schneider, R. F. Boisvert, C. W. Clark, B. R. Miller, B. V. Saunders, H. S. Cohl, and M. A. McClain, eds.
- [43] Petter Kolm, Shidong Jiang, and Vladimir Rokhlin. Quadruple and octuple layer potentials in two dimensions i: Analytical apparatus. *Applied and Computational Harmonic Analysis*, 14(1):47–74, 2003.
- [44] David Colton and Rainer Kress. *Inverse Acoustic and Electromagnetic Scattering Theory*. Number 93 in Applied Mathematical Sciences. Springer, 3rd ed. 2013 edition, 2013.
- [45] E.B Fabes, Max Jodeit, and J.E Lewis. On the spectra of a hardy kernel. *Journal of Functional Analysis*, 21(2):187–194, 1976-02.
- [46] Michael O’Neil. Second-kind integral equations for the laplace-beltrami problem on surfaces in three dimensions. *Advances in Computational Mathematics*, 44(5):1385–1409, 2018.
- [47] Jean-Claude Nédélec. *Acoustic and Electromagnetic Equations: Integral Representations for Harmonic Problems*. Number 144 in Applied Mathematical Sciences. Springer, 2001.
- [48] Thierry Aubin. *Nonlinear Analysis on Manifolds. Monge-Ampère Equations*, volume 252 of *Grundlehren der mathematischen Wissenschaften*. Springer New York, 1982.
- [49] Thierry Aubin. Espaces de sobolev sur les variétés riemanniennes. *Bulletin des Sciences Mathématiques*, 100:149–173, 1976.
- [50] Tristan Goodwill, Leslie Greengard, Jeremy Hoskins, Manas Rachh, and Yuguang Wang. Fast multipole method with complex coordinates, 2025.
- [51] Alex Barnett and Leslie Greengard. A new integral representation for quasi-periodic scattering problems in two dimensions. *BIT Numerical mathematics*, 51(1):67–90, 2011.
- [52] Adrianna Gillman, Alex H Barnett, and Per-Gunnar Martinsson. A spectrally accurate direct solution technique for frequency-domain scattering problems with variable media. *BIT Numerical Mathematics*, 55(1):141–170, 2015.
- [53] Travis Askham, Manas Rachh, Michael O’Neil, Jeremy Hoskins, Daneil Fortunato, Shidong Jiang, Fredrik Fryklund, Tristan Goodwill, Hai Yang Wang, and Hai Zhu. chunkIE: a MATLAB integral equation toolbox, 2024.
- [54] J. Ma, V. Rokhlin, and S. Wandzura. Generalized gaussian quadrature rules for systems of arbitrary functions. *SIAM Journal on Numerical Analysis*, 33(3):971–996, 1996.
- [55] James Bremer, Zydrunas Gimbutas, and Vladimir Rokhlin. A nonlinear optimization procedure for generalized gaussian quadratures. *SIAM Journal on Scientific Computing*, 32(4):1761–1788, 2010.
- [56] Felipe Vico, Leslie Greengard, Michael O’Neil, and Manas Rachh. A fast boundary integral method for high-order multiscale mesh generation. *SIAM Journal on Scientific Computing*, 42(2):A1380–A1401, 2020.